



# Thermal and kinetic behaviors of pyrolytic carbon black and gas coal in co-combustion

Qi Wang<sup>1</sup> · Guangwei Wang<sup>1</sup> · Jianliang Zhang<sup>1</sup> · Haiyang Wang<sup>1</sup>

Received: 29 August 2018 / Accepted: 17 November 2018 / Published online: 30 November 2018  
© Akadémiai Kiadó, Budapest, Hungary 2018

## Abstract

In this study, a combustion study of tire pyrolytic carbon black (CBp), gas coal (GC), and their blends was carried out by thermogravimetric analysis with four heating rates under air atmosphere. And the structure characteristics of CBp and GC were studied using particle size distribution, scanning electron microscope, X-ray diffraction, Raman spectra followed by peak deconvolution and data analysis. The results demonstrated that the structural differences between CBp and GC directly affected their thermal behavior trends. GC with low graphitization degree had more combustibility reactivity than that of CBp, while the mean reaction rate and maximum reaction rate of CBp were larger than GC due to its bigger specific surface area and higher porosity. For blends, the combustibility reactivity could be improved by blending with GC, and there was obviously synergetic effect for the co-combustion of CBp and GC. The combustion reaction mechanisms and kinetic parameters were carried out using three non-isothermal kinetic models: random nucleation nuclei growth model (RNGM), volume reaction model, and unreacted core model. The kinetic analysis demonstrated that the RNGM model had a better performance than other models for describing the thermal behavior of the selected samples. In addition, the synergetic effect between CBp and GC was observed from the kinetics data calculated by RNGM. The activation energies of CBp and GC calculated by RNGM model were 119.6 kJ mol<sup>-1</sup> and 126.4 kJ mol<sup>-1</sup>, respectively, whereas the lowest activation energy for their blends was 104.3 kJ mol<sup>-1</sup> when CBp ratio was 40%.

**Keywords** Combustibility · Thermogravimetric · Kinetics models · Pyrolytic carbon black

## Introduction

Along with the continuing fast growth in Chinese economy and the successive increase in people's living standard, the automobile industry enters into a fast-growing era. Rapidly developing industry has brought great convenience to people's life, but at the same time, it also brings an increase in waste tires' number [1]. According to an incomplete statistic, approximately 400 million tires are discarded around China annual by 2016, and this figure is estimated to increase by 8–10% every year [2]. The waste tires not only cause the waste of land resources, but also have a series of negative effects such as fire and more, and more

“Black Pollution” [3–5] formed by waste tires is gradually threatening the human living environment.

At present, the recycling of waste tires has broken the ice in China. There are three main forms of recycling waste tires. The first form of recycling waste tire is renovation and reuse. However, there is a large gap between China and developed countries in refurbishment rate of tires due to slow retreading technology, defective management system, bad recycling channels, low user trust, and so on. The average proportion of refurbished tires in the world is 10:1, while it is only 26:1.5 in China [6]. The second form of recycling waste tire is making crumb rubber. According to the statistical data of China Rubber Industry Association, China's powder application is more than 50,000 t, but there is still 50% rubber powder without market compared with the 100,000–120,000 t annual output of rubber powder in China [7]. The third form recovers waste tires by non-stripping micro-negative pressure pyrolysis [8]. In this way, waste tires are divided into about 45% fuel oil, 35%

✉ Guangwei Wang  
wgw676@163.com

<sup>1</sup> School of Metallurgical and Ecological Engineering,  
University of Science and Technology, Beijing 100083,  
China

carbon black, 10% combustible gas and 10% wire [9]. The waste steel wire, as a high-quality wire scrap, is the high-quality raw material for steelmaking. The combustible gas can be directly used in the pyrolysis reactor as the heat source by efficient recovery technology [10]. The calorific value of chemical oil is about 9700 thousand calories, which can supply boilers and industrial furnaces as fuel oil. However, the untreated pyrolytic carbon black can only be used as low industrial filler due to its high ash content and poor surface activity [11].

In order to effectively recover the heat in waste tires, Michelin and Arcelor [12] have carried on the long-term deep research on injecting scrap tire into the electric furnace for steelmaking, and the industrial experiments were successful. The Nippon Steel Smoke Plant [13] in Japan is a successor to use waste tires instead of pulverized coal as a carbon source and heat source for scrap-melting furnaces. The Norfolk company [14] in America is working on a process to spray waste tires into electric arc furnaces to provide chemical energy to molten steel. However, the injection of waste tires into the blast furnace has not been widely promoted and applied in China due to the poor grinding ability. Pyrolysis carbon black has good grinding ability and high calorific value, and it is possible to use pyrolysis carbon black with bituminous coal to provide the heat for industrial production, which can utilize the characteristics of unique combustibility of bituminous coal and also use the characteristics of high fix carbon content and high calorific value of carbon black. In China, technological advances and industry growth have become possible with the unreasonable consumption of the coal resources. Although China is rich in coal reserves, a large amount of long-term consumption will lead to lack of resources. Therefore, it is necessary to explore new carbon-containing fuels instead of coal. Thermogravimetric analyzer, fluidized bed reactor, mass spectrometry analyses, and tube reactor are the frequently used techniques for the investigation of combustion of biomass and coal [15–18], waste plastics and coal [19–22], and blast furnace flue dust and coal [23]. To date, complete kinetic research on carbon black and coal have not been found.

In this paper, the combustion characteristics and kinetic behaviors of GC, CBp, and their blends were investigated by a non-isothermal thermogravimetric analysis method under air atmosphere. In order to explain the different thermal behavior trends of these samples, various factors including particle size analyzer, scanning electronic microscopy, XRD, and Raman spectra were studied to reflect structure characteristic. Then three nth-order representative gas–solid models: random nucleation nuclei growth model (RNGM) [24, 25], volume reaction model (VM) [26], and unreacted core model (URCM) [27, 28], were employed to calculate kinetic parameters that could

explain the combustion process of CBp, GC, and their blends. It is hoped that this paper will be conducive to understand the combustion process of tire pyrolytic carbon black and provide a basic to use tire pyrolytic carbon black for blast furnace or thermo-power station.

## Experimental

### Raw materials

In this study, Chinese gas coal (GC) and pyrolytic carbon black (CBp) were selected for this investigation. China is rich in the GC resources, but GC is injected into the blast furnace only after it has been upgraded or mixed with anthracite due to its low carbon content and calorific value. The CBp is provided from a waste-tire-processing plant in China. Because of the backward equipment and technology, the CBp produced by this plant can only be used as industrial filler. All raw materials were dried at 105 °C, and the particle size of the materials is < 74 μm. Proximate analysis and ultimate analysis results of GC and CBp are given in Table 1.

### Experiment procedure

#### Thermogravimetric analysis

The combustion experiments were carried out in a TG (Setaram Labsys-Evo) under air atmospheric. About 5 mg of the samples was burned at four heating rates of 2.5, 5, 10, and 20 °C min<sup>-1</sup> from room temperature to 900 °C, respectively. The small amount of sample, air flow, and slow heating rates were selected, after some preliminary tests, in order to ensure the heat transfer limitations can be ignored.

#### Microstructure test

The particle size distribution of the GC and CBp was determined by LMS-30 scattering laser diffraction particle size analyzer. The microscopic morphology of the samples was carried out using a Quanta 250 environmental scanning electron in a secondary electron emission mode.

**Table 1** Proximate and ultimate analysis of GC and CBp

Sample	Proximate analysis/%			Ultimate analysis/%				
	FC <sub>d</sub> <sup>a</sup>	A <sub>d</sub>	V <sub>d</sub>	C <sub>d</sub>	H <sub>d</sub>	O <sub>d</sub> <sup>a</sup>	N <sub>d</sub>	S <sub>d</sub>
GC	60.3	10.4	29.4	78.9	4.9	4.8	0.7	0.3
CBp	77.7	14.5	7.8	78.3	1.6	2.6	0.3	2.7

## Raman spectroscopy

The Raman spectra of the samples were obtained with a JY-HR800 spectrometer. Experiments were examined at room temperature using wavelength 532 nm (10 s, 20 mw) provided by HE-NE laser, and any annealing effects were considered negligible. In order to avoid accidental errors, the spectra were obtained from several particles of each sample and recorded in the range 800–2000 cm. The acquisition time of each spectroscopy was 60 s, and the spectra were subject to peak fitting using curve-fitting software (Peak Fitting Module).

## X-ray diffraction

The crystal structure of the samples was obtained using X-ray diffraction (XRD) analysis. X-ray diffraction carried a MAC Science X-ray powder diffractometer (M21XVHF22) with a Cu K $\alpha$  radiation source ( $\lambda = 1.54051 \text{ \AA}$ ). Diffraction intensities were recorded in the  $2\theta$  range of  $10^\circ$ – $90^\circ$  in a step-scan mode.

## Kinetic model

Three well-known non-isothermal kinetic models including RNGM, VM, and URCM models were adopted in this study to calculate the kinetic parameters of CBp, GC, and their blends. The combustion process of GC, CBp, and their blends are gas–solid non-catalytic heterogeneous reaction generally described as:

$$\frac{dX}{dt} = k(P_g, T)f(X), \quad (1)$$

where  $k$  is apparent reaction rate constant, which is a function of partial pressure  $P_g$ , and reaction temperature  $T$ .  $f(X)$  describes a kinetic mechanism function in the combustion process,  $X$  is conversion degree which can be defined as:

$$X = \frac{w_0 - w_t}{w_0 - w_f}, \quad (2)$$

where  $w_0$ (mg) denotes the original mass of the sample,  $w_t$  (mg) is the mass at time  $t$  and  $w_f$  is the final mass at the end of combustion. It is assumed that solid fuel combustion is a first-order reaction and can be expressed using the Arrhenius equation, which gives:

$$\frac{dX}{dt} = k_0 e^{-E/RT} f(X), \quad (3)$$

where  $k_0$  is pre-exponential factor,  $E$  stands activation energy,  $R$  is the universal gas constant. The RNGM model takes into account the pore structure and evolution during

the reaction development. And the RNGM model can express as:

$$\frac{dX}{dt} = k_0 e^{-E/RT} (1-X) \sqrt{-(1-X)} \quad (4)$$

The VM model supposes that the reaction is evenly produced on both the outside and inside solid particle surface. The VM model is given by following equation:

$$\frac{dX}{dt} = k_0 e^{-E/RT} (1-X). \quad (5)$$

The URCM model assumes that the reaction occurs gradually from particle surface to inside and that there is always a shrinking core of non-reacted solid during the reaction. The reaction mechanism function is given by following equation:

$$\frac{dX}{dt} = k_0 e^{-E/RT} (1-X)^{2/3} \quad (6)$$

For non-isothermal conditions, the experimental temperature  $T$  is determined by constant heating rate  $\beta$  and the reaction time  $t$ :

$$T = T_0 + \beta t \quad (7)$$

The RNGM model is given as follows by introducing Eq. (7) into Eq. (4):

$$X = 1 - \exp\left(-\left(-\frac{k_0(T-T_0)}{2\beta} \cdot \exp\left(-\frac{E}{RT}\right)\right)^2\right). \quad (8)$$

Similarly, the VM model is given as follows by introducing Eq. (7) into Eq. (5):

$$X = 1 - \exp\left(-k_0 \frac{(T-T_0)}{\beta} \cdot \exp\left(\frac{-E}{RT}\right)\right). \quad (9)$$

And URCM model is obtained by integrating Eq. (7) to give Eq. (6):

$$X = 1 - \left(1 - \frac{k_0(T-T_0)}{3\beta} \cdot \exp\left(\frac{-E}{RT}\right)\right)^3. \quad (10)$$

The kinetic parameters were carried out using nonlinear least-squares fitting method. In order to further verify the three models quantitatively, the experimental and calculated values were compared by the following equation:

$$\text{DEV}(X)(\%) = 100 \times \sqrt{\frac{\sum_{i=1}^N (X_{\text{exp},i} - X_{\text{calc},i})^2}{N}} \quad (11)$$

DEV ( $X$ ) (%) is relative error, and its value can represent the effect of model fitting;  $X_{\text{exp},i}$  is experimental data obtained from TG;  $X_{\text{calc},i}$  is a value fitted by three models;  $N$  is the number of experiment data.

## Results and discussion

### Thermal combustion of raw materials and their blends

It is generally accepted that the combustion process of carbon includes three main stages: (1) first stage: moisture drying and gas absorption; (2) second stage: devolatilization and combustion of fixed carbon up to the largest mass loss; (3) third stage: combustion is completed and the mass losses of the samples remained unchanged. It is observed that there are similar three stages in the TG results of GC, CBp and their blends at different heating rates depicted in Fig. 1. All TG curves (TG–DTG) are selected from 200 °C due to minor mass losses associated with the removal of moisture in the initial period. According to the curves, the mass losses mainly occurred at 300–600 °C, and DTG curves have only one peak rate for all raw materials and mixtures. In addition, the TG curve of select samples moves to a high-temperature area with an increase in heating rate. This is because of the fact that combustion reactions of CBp, GC, and their blends are all endothermic, and so more time is needed to transfer heat to low internal temperature of these samples under high heating rates.

In order to describe the combustion process of the selected samples in more detail, TG–DTG [29] method is carried out to calculate combustion parameters of CBp, GC, and their blends. Ignition temperature  $T_i$ , burn out temperature  $T_f$ , mean reaction rate  $R_{\text{mean}}$ , maximum reaction rate  $R_{\text{max}}$ , comprehensive combustion index  $S$  ( $S = \frac{R_{\text{max}}R_{\text{mean}}}{T_i^2T_f}$ ) [30] under 10 °C/min heating rate are shown in Table 2. From combustion parameters, it is observed that the values of  $T_i$  and  $T_f$  of GC are lower than that of CBp and  $T_i$  and  $T_f$  for blends lie in the range between the two samples. With increase in CBp content,  $R_{\text{mean}}$  and  $R_{\text{max}}$  for blends first decreases and then increases. The lowest value of  $R_{\text{mean}}$  and  $R_{\text{max}}$  for blend is 0.0974 min obtained at 40% of CBp content. For comprehensive combustion index  $S$ , similar relation can be found. From above analysis, it can be found that the blend has good ignition property as the content of GC increases in the mixture, while it is deteriorated with the mixture of two samples for comprehensive combustion characteristics, especially when blend is GC60%/CBp40%. This phenomenon is caused by different combustion intervals of CBp and GC. GC has low  $T_i$ , and for separate combustion, it is concentrated in the low-temperature region, while CBp has high  $T_f$  and burns in high-temperature region compared to GC. However, when CBp and GC are mixed together, the concentrated combustion range will be extended and strength will be weak. Similar phenomena are also found in

thermal behavior of coal and paper mill sludge in co-combustion by Liao and Ma [31].

It is observed that after mixing of CBp and GC, combustion process of blends becomes more complicated. In order to determine whether there is a synergistic effect in the process of co-combustion, the average conversion value of GC conversion and CBp conversion in the combustion process is compared with the experimental data. It is generally accepted that the effect is positive when the calculated value is lower than experiment data, while there is a negative effect when the calculated value is higher than the experiment data. It is considered that there is no synergistic effect in the co-combustion process when calculated value is same with experiment data. Consequently, the difference between calculated and experiment data directly reflects the synergistic effect in co-combustion. Supposing there is no interaction between GC and CBp, massed average of single sample represents the overall mass loss of the blends that is expressed by Eq. (12):

$$X_{\text{calculate}} = a \times X_{\text{GC}} + b \times X_{\text{CBp}} \quad (12)$$

Figure 2 shows the comparisons between calculated and experiment data. From the curves, it is obviously seen that experiment curve is similar to calculated curve, but there are also deviations at different stages. In the range of 400–500 °C, experiment data are obviously lower than calculated value. Then experiment data become higher than calculated data in the range 500–550 °C. At the end of the combustion process, experiment data and calculated data become close with each other. All above results reflect that synergistic effect is present. It is well known that volatilization and combustion of volatile content occur at the initial stage of combustion. For blends, this process is limited by mixing of GC and CBp. More temperature is needed for volatile content to evaporate due to small amount of volatile matter and high coalification degree of CBp. When CBp and GC are mixed and burned, different particles will limit heat transfer, resulting in an increase in temperature gradient. These limits caused the volatilization and combustion of volatile content into high temperature range. With the raising combustion temperature, carbon residue begins to burn. For the combustion of carbon residue, solid carbon from GC promotes combustion of char in CBp. This can be explained as: The ignition temperature of solid carbon from GC is low, and so it is easy to burn and release a lot of heat that can promote the combustion of char in CBp. According to above analyses, it can be concluded that the content of CBp limits volatilization of volatile content in GC and combustion of solid carbon in GC can obviously promote combustion of char in CBp.

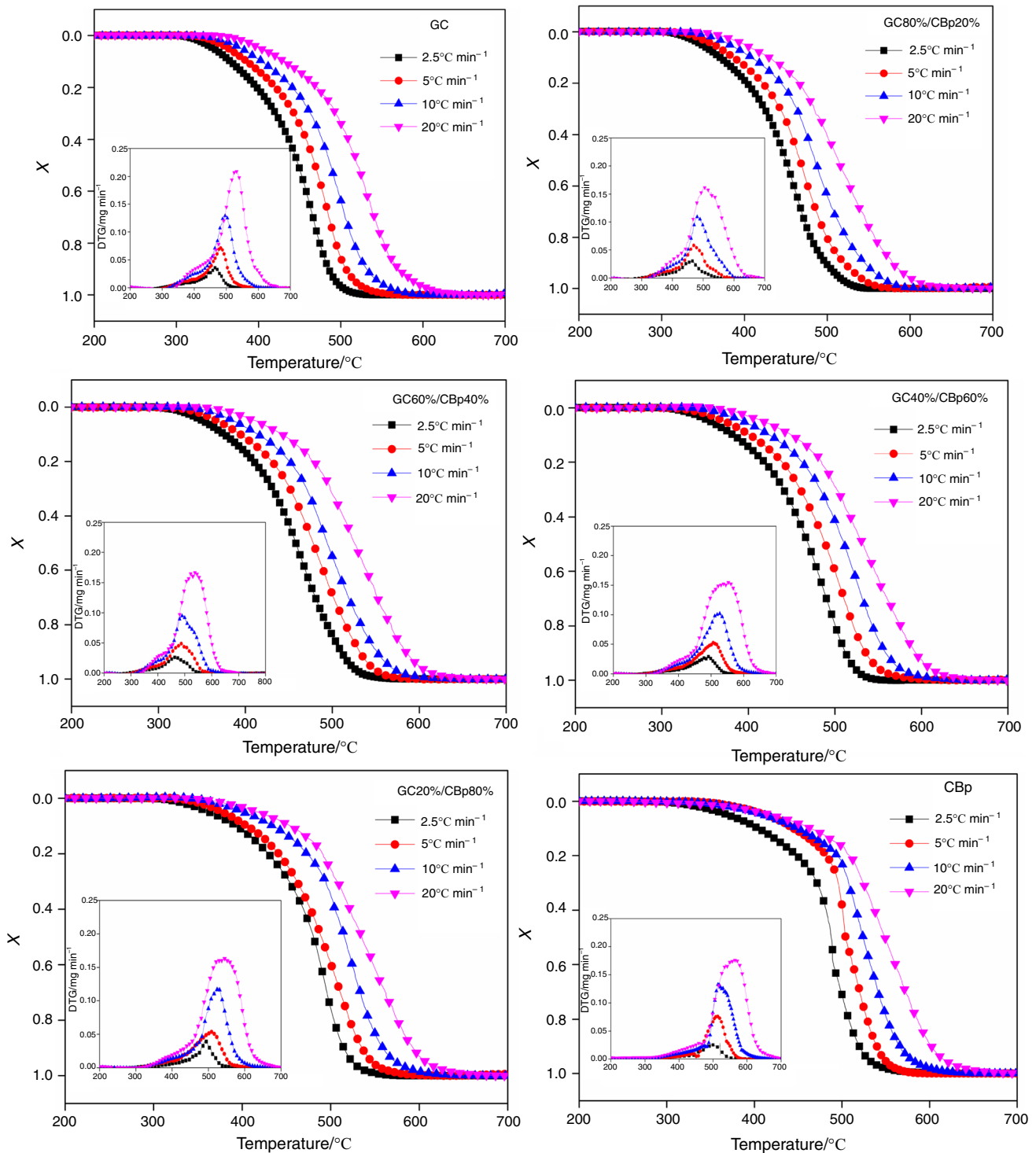


**Fig. 1** Conversion and conversion rate of GC, CBp, and their blends at four different heating rates

### Physical and chemical characteristics

The particle size of GC and CBp samples is shown in Fig. 3. It can be observed that the particle size of GC is between 2 and 65  $\mu\text{m}$ , while that of CBp is between 2 and 27  $\mu\text{m}$ . The particle size of CBp is smaller than GC. The

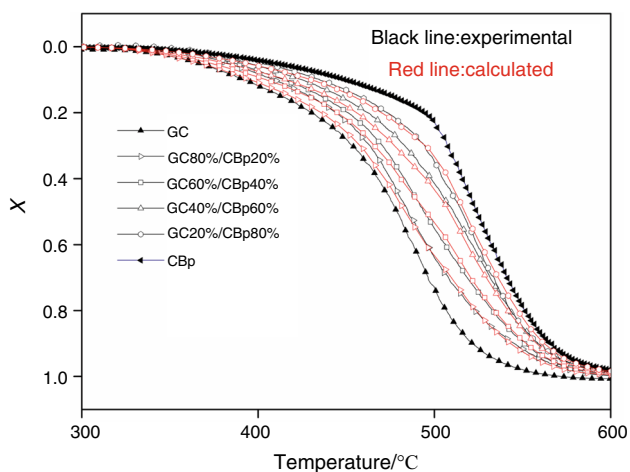
specific surface area is obtained by calculating the original data of the particle size distribution. The specific surface area of CBp is  $1.019 \text{ m}^2 \text{ cm}^{-3}$ , and specific surface area of GC is  $0.710 \text{ m}^2 \text{ cm}^{-3}$ .

The surface microtopography of GC and CBp was obtained by scanning electron microscopy (SEM) and is



**Table 2** Representative combustion parameters of GC, CBp, and their blends at  $10\text{ }^\circ\text{C min}^{-1}$  heating rates

Sample	$T_i/^\circ\text{C}$	$T_f/^\circ\text{C}$	$R_{\text{mean}}/\text{min}$	$R_{\text{max}}/\text{min}$	$s \times 10^{11}$
GC	374.2	548.2	0.0363	0.1321	6.25
GC80%/CBp20%	379.4	561.6	0.0304	0.1123	4.22
GC60%/CBp40%	386.5	565.0	0.0301	0.0974	3.47
GC40%/CBp60%	390.1	570.8	0.0329	0.1027	3.89
GC20%/CBp80%	398.2	573.9	0.0354	0.1196	4.65
CBp	415.5	579.4	0.0408	0.1335	5.45

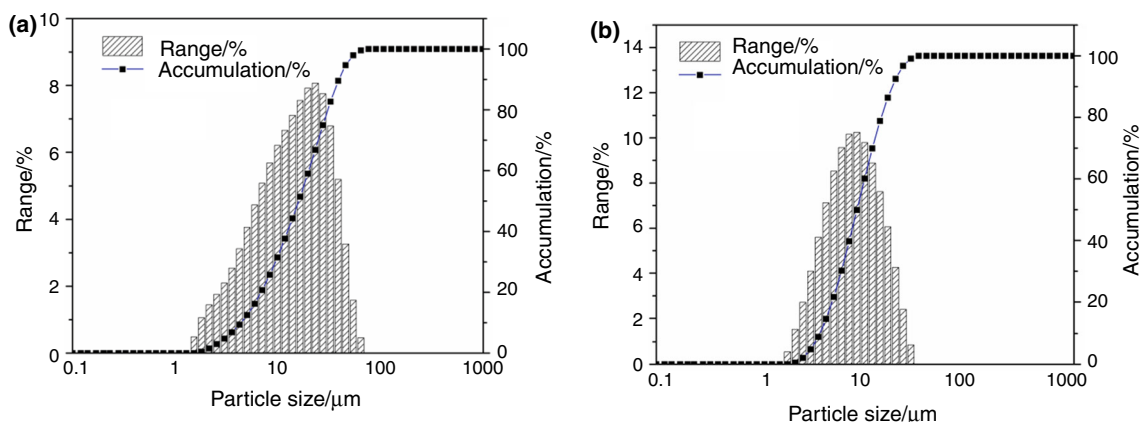
**Fig. 2** Comparison of experiment data with the calculated value ( $10\text{ }^\circ\text{C min}^{-1}$ )

shown in Fig. 4. From Fig. 4, obvious difference among the samples can be seen. The GC sample that exists in particle has smooth surfaces, sharp edges, and irregular shapes, while the surface microstructure of CBp shows a “pit-shell” structure. The internal structure of CBp is as dense and smooth as GC, and the surface layer and surface pore of CBp are formed due to the deposition of ash, the

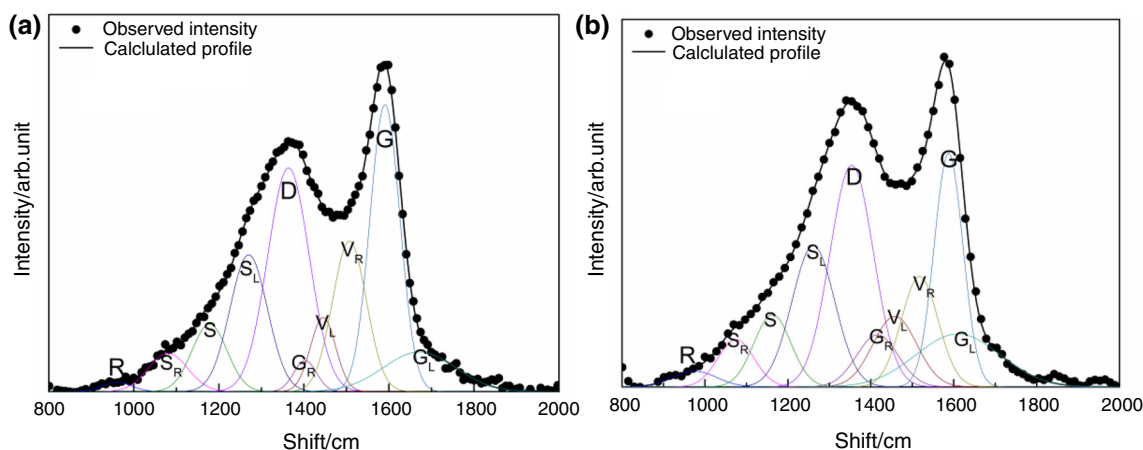
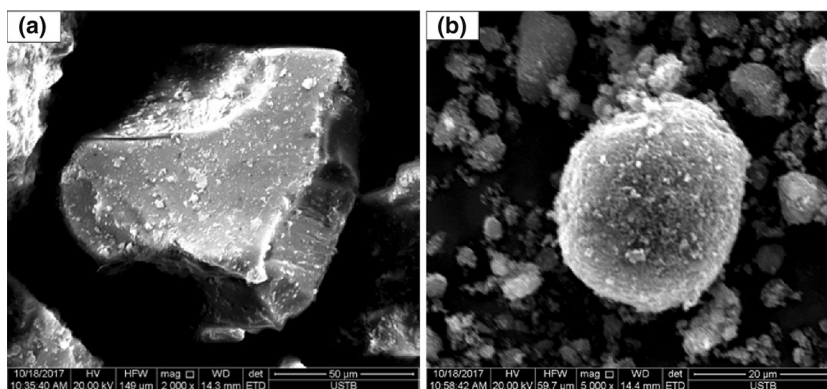
sediment of carbonaceous, and the change of surface group. In the pyrolysis process of waste tire, the precipitation of volatiles leads to its porous structure and large specific surface area. Aranda et al. also reported that solid phase of carbon black shows a porous structure [32].

Figure 5 shows the Raman spectra of CBp and GC in the range of 800–2000 cm. A deconvolution method [33] is adopted to obtain the structure parameters including peak position, full width at half maximum (*FWHM*), intensity (*I*), and integrated area (*A*). In the deconvolution method, the Raman spectra is divided into 10 Gaussian peaks including four groups/bands (*G*, *D*,  $G_R + V_L + V_R$ , and *S*) with the rest of the bands ( $G_L$ ,  $S_L$ ,  $S_R$ , and *R*) as the curve-fitting residuals. The aromatic ring breathing will contribute to the *G* band of the Raman spectrum and *D* band of the Raman spectrum is mainly caused by the aromatics containing six or more fused benzene rings. Therefore, the value of  $A_D/A_G$  can reflect the degree of aromatic ring growth. Therefore, the ratio of big rings to small fused rings can be reflected by the values  $A_D/(A_{G_R} + A_{V_L} + A_{V_R})$ . The rest of bands (*S*,  $G_L$ ,  $S_L$ ,  $S_R$ , and *R*) virtually represent cross-linking density and substitutional groups, carbonyl C=O structure, ether, benzene related, benzene accompanied structures, respectively [34]. Table 3 presents the structure parameters of CBp and GC obtained from the Raman spectra. The ratio  $A_D/A_G$  of CBp in Table 3 is distinctly smaller than that of GC, indicating that more aromatic ring growth in CBp than that in GC and the carbon crystalline structure in CBp is more ordered than that in GC. The larger ratio  $A_D/(A_{G_R} + A_{V_L} + A_{V_R})$  of CBp suggests that there are less amorphous carbon structures in CBp than that in GC. Less benzene related in CBp can be seen from the smaller ratio  $A_{S_L}/A_G$ , and the smaller ratio  $A_S/A_G$  of CBp can reflect that the cross-linking density and the degree of substitution of carbon in CBp are reduced [35].

X-ray diffraction is an important method to determine the structure of carbonaceous materials, and the structure

**Fig. 3** Particles diameter distribution of different samples: **a** GC and **b** CBp

**Fig. 4** SEM photographs of the samples: **a** GC and **b** CBp

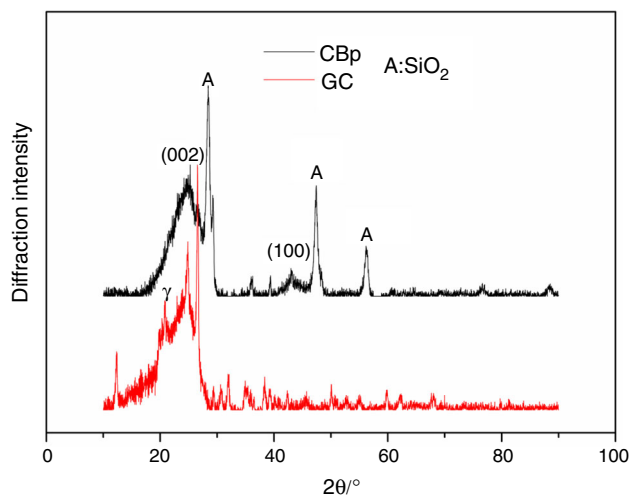


**Fig. 5** Raman spectra deconvolution using the 10 bands for selected samples at temperature: **a** CBp, **b** GC

**Table 3** Structure parameters of Raman spectrum of CBp and GC

Samples	$A_D/A_G$	$A_D/(A_{G_R} + A_{V_L} + A_{V_R})$	$A_{S_L}/A_G$	$A_S/A_G$
CBp	1.08	1.21	0.59	0.28
GC	1.43	1.03	0.90	0.39

characteristic such as aromatic structure size, atom distribution, bond length, and array can be received [31]. Three carbon peaks usually exist in the XRD curve of coal, indexed as (002), (100), and  $\gamma$ . The (002) band at around  $26^\circ$  generally indicates the stack spacing of aromatic ring layers, and  $\gamma$  band at around  $16^\circ$ – $23^\circ$  reflects the packing distance of saturated structures such as condensed saturated rings or aliphatic side chains, while (100) band at around  $44^\circ$  is associated with the hexagonal structures. X-ray diffraction profile of CBp and GC samples is shown in Fig. 6. It can be seen from the figure that there are some characteristic peaks of minerals near the carbon-based peaks, main minerals present are quartz. Because of much ash in CBp, the characteristic peak intensity of quartz in CBp is higher than that in GC. There are obvious two peaks in the XRD spectrums of CBp and GC, namely the (002)

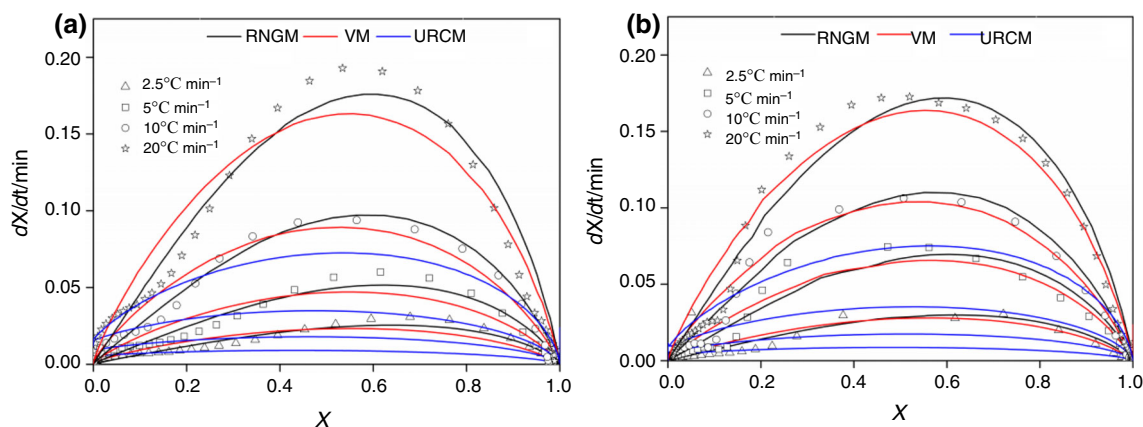


**Fig. 6** XRD spectrum of CBp and GC

band and (100) band. The degree of (002) band are the same, while the shape of the peak of CBp is steeper than that of GC, which indicated that the order degree of aromatic carbon layer in CBp is more than that of GC, and less aliphatic side chains in CBp. The (100) band at  $44^\circ$  was not clearly observed probably in GC curve due to its high

**Table 4** Microcrystalline parameters of CBp and GC samples

Sample	$2\theta_{002}/\text{deg}$	$2\theta_{100}/\text{deg}$	$B_{002}/\text{deg}$	$d_{002}/\text{\AA}$	$L_c$	$L_a$	$f_a(\text{X-ray})$	Nave
CBp	24.72	43.42	4.82	3.59	16.68	8.02	0.78	5.64
GC	24.48	42.54	5.27	3.63	15.25	8.73	0.52	5.20

**Fig. 7** Fractional conversion rate to conversion simulated by three kinetic models: **a** GC and **b** CBp

levels of background. The absence of (100) band indicates that GC have small  $L_a$  values and low levels of growth in the basal planes of graphite structures. The interlayer spacing between aromatic sheets ( $d_{002}$ ), average crystallite stacking height ( $L_c$ ), diameter ( $L_a$ ), the average number of layers ( $N$ ) in crystalline, the corresponding aromaticity ( $f_a(\text{X-ray})$ ) is calculated according to Scherrer equation [36–38]. The calculated results of crystalline structure parameters of CBp and GC are given in Table 4. Table 4 shows that the interlayer spacing ( $d_{002}$ ) of the crystallite in CBp and GC are 3.59 and 3.63, and these values are higher than those for pure graphite (3.354 Å), indicating a relatively open structure in CBp and GC [39]. The  $L_c$  of the layer structures in CBp is higher than that in GC, and the  $d_{002}$  of the crystallite structure in CBp is lower than that in GC, and it can reflect that aromatic carbon lamellas of CBp are stacked higher than that of GC. From the larger Nave in crystalline and the higher  $f_a(\text{X-ray})$  of CBp, it can infer that aromatic nucleus in CBp are more orderly arrayed. Because CBp is prepared in the condition of slow pyrolysis and its aromatic side chains have enough time to be broken and removed, the graphite degree of CBp is higher than GC. From the above, it can be seen that the graphite degree of CBp is higher than GC that consistent with Raman's results.

### Correlation between combustibility and structure characteristics

From the comparison of TG curves, it can be noted that pyrolytic carbon black and coal materials have different

thermal behavior trends. In addition, there is also big gap in physical and chemical between GC and CBp. It can be inferred that the thermal behavior trends of CBp and GC are affected by structural differences between them.

It generally accepted that the basic structural features of carbon in carbon microstructures are quite similar, while differences existed mainly in peripheral matters like volatiles matter, aliphatic chains between structural units, degree of graphitization. From combustion rate data in Table 2, the value  $T_i$  and  $T_f$  of GC is lower than that of CBp, which is related to composition and graphite degree of carbonaceous materials. As shown in Table 1, GC has much higher volatile content than CBp, whereas the fixed carbon content of GC is lower. In addition, GC has higher content of hydrogen and oxygen than that of CBp, indicating that GC easier to achieve ignition. Furthermore, the Raman results show that more aromatic ring growth, less amorphous carbon structures and less benzene related in CBp than that in GC, and the cross-linking density and the degree of substitution of carbon in CBp are small. Based on the results mentioned by XRD, it can be seen that layer structures in CBp is higher than that in GC, the crystallite structure in CBp is lower than that in GC, the aromatic nucleus in CBp are more orderly arrayed. These results reflect that open structure in GC makes it easy to burn and have lower value of  $T_f$  than that of CBp.

Wu et al. [40] reports that the larger the specific surface area of the sample, the higher the reaction rate. According to laser particle size analyzer described in Fig. 3, CBp has a larger specific surface area due to its smaller particles. From the SEM analyzer shown in Fig. 4, the pore structure



**Table 5** Calculated kinetic parameters of different samples

Samples	RNGM			VM			URCM		
	$k_0/s$	$E/kJ\ mol^{-1}$	$R^2$	$k_0/s$	$E/kJ\ mol^{-1}$	$R^2$	$k_0/s$	$E/kJ\ mol^{-1}$	$R^2$
GC	2.14E+08	119.6	0.9997	2.31E+07	131.2	0.9992	5.47E+06	104.1	0.9869
GC80%/CBp20%	1.33E+08	111.5	0.9998	3.45E+07	127.8	0.9994	3.19E+06	100.6	0.9728
GC60%/CBp 40%	8.64E+07	104.3	0.9999	8.94E+06	119.2	0.9995	1.23E+05	93.7	0.9745
GC 40%/CBp 60%	3.47E+07	109.2	0.9997	6.72E+06	125.4	0.9991	3.43E+05	99.2	0.9862
GC 20%/CBp 80%	1.19E+08	115.2	0.9995	5.67E+06	128.6	0.9993	7.81E+05	103.4	0.9774
CBp	3.24 E+08	126.4	0.9988	6.87E+07	135.2	0.9974	3.45E+06	110.8	0.9548

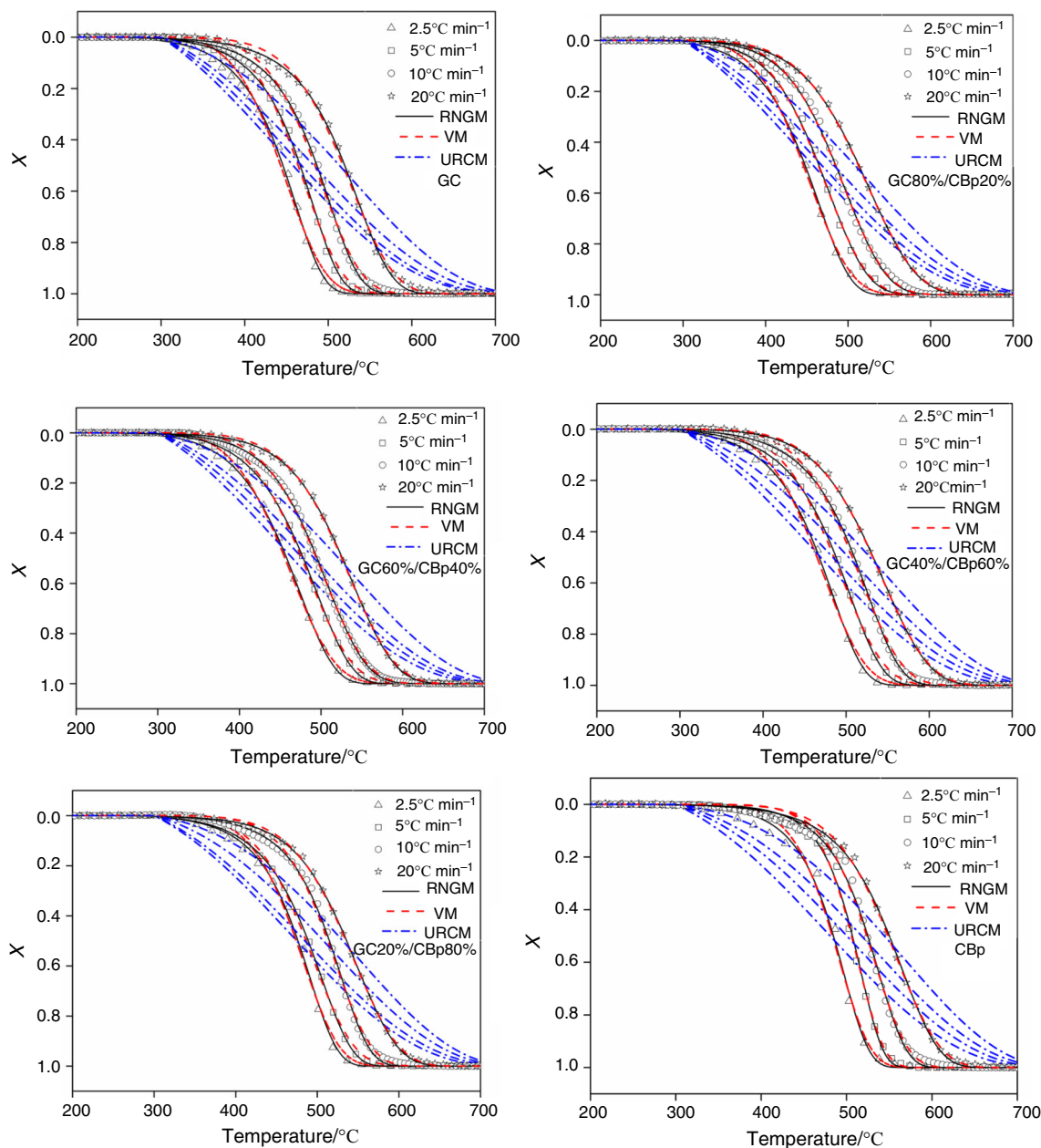


**Fig. 8** Fitting curves to the nonlinear fitting method for CBp, GC and their blends

of CBp is more developed than that of GC. The larger specific surface area and pore structure afford a good condition for carbon in CBp to react with oxygen. Therefore, the mean reaction rate  $R_{\text{mean}}$  and maximum reaction rate  $R_{\text{max}}$  of CBp are larger than those of GC.

### Kinetic analysis

Figure 7 shows the relations of conversion rate and conversion of GC and CBp calculated by three kinetic models. From the curves, it can be found that the conversion rate first increases and then decreases with the increase in conversion. This can be explained as: at the initial period of reaction, the surface area and active sites of the samples can improve the conversion rate. When the reaction process reaches a certain level, the surface area and active site of the sample remain constant despite the temperature rising further. Furthermore, kinetic models not fit well under the condition of  $20\text{ }^{\circ}\text{C min}^{-1}$  heating rate, revealing that thermal hysteresis at high heating rate is serious.

In order to determine the effect of the mixing ratio on the combustion kinetics parameters (pre-exponential factor and activation energy) of GC and CBp, the RNGM, VM, URCM models are used. Based on Eqs. (8), (9), and (10), the kinetic parameters of the selected samples are carried out using nonlinear fitting method and results are given in Table 5. Figure 8 show the fitting curves to the nonlinear fitting method for CBp, GC, and their blends. It is shown that fitting profiles of CBp, GC, and their blends by URCM model was far from experimental ones and RNGM model displays a significant fit (the highest  $R^2$  value). It is well known that RNGM model supposes that particles contain a number of pores structures whose shape is assumed cylindrical and surface area varies with the increase in conversion. The VM model assumes that the particle size remains constant, and the density changes uniformly as the particle reacts on the entire surface. The URCM model assumes that the reaction occurs gradually from particle surface to inside, and there is always a shrinking core of non-reacted solid during the reaction [41]. According to the SEM images, shapes of pore structure in CBp are deformed and not even, it can be inferred that structure factor have little effect on reaction and Eq. (8) is approximately equal to Eq. (9). Therefore, the RNGM and VM models give similar results in Fig. 8. By analyzing the change of activation energies of different samples with varied CBp ratio, it can be concluded that activation energy decreases and then increases with the increase in CBp ratio. When the CBp ratio is 40%, the least value of the activation energy for the blends is  $104.3\text{ kJ mol}^{-1}$ . This phenomenon indicates that there is an obviously synergetic effect between CBp and GC co-combustion. The synergetic effect has been detailed discussed in Sect. 3.1. It is generally

**Table 6** Deviation between experimental and calculated data

Samples	DEV (X)/%		
	RNGM	VM	URCM
GC	1.23	1.31	6.11
GC80%/CBp20%	0.89	0.94	7.07
GC60%/CBp 40%	0.74	0.83	6.83
GC 40%/CBp 60%	1.15	1.22	7.46
GC 20%/CBp 80%	1.33	1.35	7.54
CBp	2.21	2.56	8.21

accepted that the lower the activation energy is, the higher reaction rate will be. However, from Table 2 it is observed that the combustion rate first decreases and then increases with the CBp matter increases, which is opposite to the variation of activation energy. In truth, activation energy and pre-exponential factor both contribute to the reaction rate. The pre-exponential factor indicates the number of collisions of the activated molecules, and it can be inferred that the greater pre-exponential factor can bring a higher the reaction rate under the same activation energy condition. For example, from Table 2, the activation energy of CBp is higher than the blends GC20% and CBp80%, but the reaction rate of CBp is also higher than the sample of GC20%/CBp80% due to the larger pre-exponential factor of CBp. This is a compensation effect named by kinetic studies, a very common study of coal gasification, biofuels, and other carbonaceous materials [42–44].

Form Fig. 8, it is obviously that there is a good accordance between calculation values and experimental data for CBp, GC, and their blends. In order to quantify the errors produced by the kinetic models in predicting the values of conversion, the deviation (DEV) described in Eq. (11) is carried out to compare the value of experimental and calculated data. The deviation obtained from three models is given in Table 6. From Table 6, it can be seen that the lowest deviation is obtained by using RNGM model for selected samples. Therefore, it can be inferred that RNGM model has a better performance than other models for describing the thermal behavior. According to above analyses, the results can provide a reference for the further establishment of mathematical models designing complicated combustion device.

### Conclusions

Co-combustion behaviors of tire pyrolytic carbon black with gas coal were investigated by thermogravimetric analysis. Results show that the structural differences between CBp and GC directly affected their thermal

behavior trends. The larger specific surface area and pore structure afford a good condition for carbon in CBp to react with oxygen. Thus  $R_{\text{mean}}$  and  $R_{\text{max}}$  of CBp is larger than that of GC. However, the results of the XRD and Raman show that the graphite degree of CBp is higher than GC, which lead GC have a lower value of  $T_i$  and  $T_f$ . Simultaneously, the kinetic parameters were obtained by three kinetic models. It can be concluded from kinetic parameters that the synergetic effect is most obvious when CBp mass ratio is 40%, the activation energies first decrease and then increase with the increase in CBp content, and it have the lowest value when CBp ratio is 40%.

**Acknowledgements** This work was supported by the Yong Elite Scientists Sponsorship Program by CAST (2017QNRC001). The authors are grateful to the Natural Science Foundation for Young Scientists of China (No. 51704019) for the financial support.

## References

- Wu B, Zhou MH. Recycling of waste tyre rubber into oil absorbent. *Waste Manag.* 2009;29:355–9.
- Ramarad S, Khalid M, Ratnam CT. Waste tire rubber in polymer blends: a review on the evolution, properties and future. *Progress Mater Sci.* 2015;72:100–8.
- Aranda A, Murillo R, Garcia T. Steam activation of tyre pyrolytic carbon black: kinetic study in a thermobalance. *Chem Eng J.* 2007;126:79–85.
- Fukumori K, Matsushita M, Okamoto H, Sato N, Takeuchi K. Recycling technology of tire rubber. *JSAE Rev.* 2002;23:259–64.
- Karger J, Mészáros L, Bárány T. Ground tyre rubber (GTR) in thermoplastics, thermosets, and rubbers. *J Mater Sci.* 2013;48:1–38.
- Zhu BZ, Cheng G, Wang Y. Review of Recycling Utilization for Waste Tire in China. *Guangzhou Chem Ind.* 2014;42:11–2.
- Li L, Liu S, Zhu T. Application of activated carbon derived from scrap tires for adsorption of Rhodamine B. *J Environ Sci.* 2010;22:1273–80.
- Aylón E, Fernández-Colino A, Murillo R. Valorisation of waste tyre by pyrolysis in a moving bed reactor. *Waste Manag.* 2010;30:1220–4.
- Frigo S, Seggiani M, Puccini M. Liquid fuel production from waste tyre pyrolysis and its utilisation in a diesel engine. *Fuel.* 2014;116:399–408.
- Li S, Wan C, Wang S. Separation of core-shell structured carbon black nanoparticles from waste tires by light pyrolysis. *Comp Sci Technol.* 2016;135:13–20.
- Li S, Wan C, Wu X. Core-shell structured carbon nanoparticles derived from light pyrolysis of waste tires. *Polym Degrad Stab.* 2016;129:192–8.
- Ware PS. Pyrolysis of waste tyres and future. *Chem Biol.* 2015;1:1–9.
- Sawada Y. Iron and steel production and technology in Japan during 2004. *ISIJ.* 2005;45:771–90.
- Allen JL, Gatz JL, Eklund PC. Applications for activated carbons from used tires: butane working capacity. *Carbon.* 1999;37:1485–9.
- Wang G, Zhang J, Chang W. Structural features and gasification reactivity of biomass chars pyrolyzed in different atmospheres at high temperature. *Energy.* 2018;147:25–35.
- Wang G, Zhang J, Zhang G. Experimental and kinetic studies on co-gasification of petroleum coke and biomass char blends. *Energy.* 2017;131:27–40.
- Wang G, Zhang J, Shao J. Experimental and modeling studies on CO<sub>2</sub> gasification of biomass chars. *Energy.* 2016;114:143–54.
- Wang G, Zhang J, Shao J. Thermal behavior and kinetic analysis of co-combustion of waste biomass/low rank coal blends. *Energy Convers Manag.* 2016;124:414–26.
- Çepelioğullar Ö, Pütün AE. Thermal and kinetic behaviors of biomass and plastic wastes in co-pyrolysis. *Energy Convers Manag.* 2013;75:263–70.
- Zhou L, Wang Y, Huang Q. Thermogravimetric characteristics and kinetic of plastic and biomass blends co-pyrolysis. *Fuel Process Technol.* 2006;87:963–9.
- Wang Q, Zhang J, Wang G. Thermal and kinetic analysis of a coal with different waste plastic (PVC) in co-combustion. *Energy Fuels.* 2018;32:2145–55.
- Ma S, Lu J, Gao J. Study of the low temperature pyrolysis of PVC. *Energy Fuels.* 2002;16:338–42.
- Zhao D, Zhang J, Wang G. Structure characteristics and combustibility of carbonaceous materials from blast furnace flue dust. *Appl Therm Eng.* 2016;108:1168–77.
- Bhatia SK, Perlmutter DD. A random pore model for fluid-solid reactions: I isothermal, kinetic control. *AIChE J.* 1980;26:379–86.
- Bhatia SK, Perlmutter DD. A random pore model for fluid-solid reactions: II diffusion and transport effects. *AIChE J.* 1981;27:247–54.
- Ochoa J, Cassanello MC, Bonelli PR. CO<sub>2</sub> gasification of argentinean coal chars: a kinetic characterization. *Fuel Process Technol.* 2001;74:161–76.
- Kasaoka S, Sakata Y, Kayano S. Kinetic evaluation of reactivity of various coal chars for gasification with carbon dioxide in comparison with steam. *Int Chem Eng.* 1984;25:160–75.
- Yuh SJ, Wolf EE. Kinetic and FTIR studies of the sodium catalyzed steam gasification of coal char. *Fuel.* 1984;63:1604–9.
- Xu YG, Zhang C, Xia J. Experimental study on the comprehensive behavior of combustion for blended coals. *Asia-Pacific J Chem Eng.* 2010;5:435–40.
- Essenhig RH, Misra MK, Shaw SW. Ignition of coal particles: a review. *Combust Flame.* 1989;77:3–30.
- Hu SC, Ma XQ, Lin YS, Yu ZS, Fang SW. Thermogravimetric analysis of the cocombustion of paper sludge and municipal solid waste. *Energy Convers Manag.* 2015;99:112–8.
- Aranda A, Murillo R, García T. Steam activation of tyre pyrolytic carbon black: kinetic study in a thermobalance. *Chem Eng J.* 2007;126:79–85.
- Li X, Hayashi J, Li CZ. FT-Raman spectroscopic study of the evolution of char structure during the pyrolysis of a Victorian brown coal. *Fuel.* 2006;85:1700–7.
- Dun W, Gujian L. Investigation of structural characteristics of thermally metamorphosed coal by FTIR spectroscopy and X-ray diffraction. *Energy Fuels.* 2013;27:5823–30.
- Li K, Khanna R, Zhang J. Comprehensive investigation of various structural features of bituminous coals using advanced analytical techniques. *Energy Fuels.* 2015;29:7178–89.
- Xu RS, Zhang JL, Wang GW. Devolatilization characteristics and kinetic analysis of lump coal from China COREX3000 under high temperature. *Metall Mater Trans B.* 2016;47:2535–48.
- Jiang JP, Luo GY, Kang JW. Study on XRD and dynamometamorphism of fault coal. *J China Coal Soc.* 2001;1:31–4.
- Wen JL, Sun SL, Yuan TQ, Xu F. Understanding the chemical and structural transformation of lignin macromolecule during torrefaction. *Appl Energy.* 2014;121:1–9.

39. Takagi H, Maruyama K, Yoshizawa N, Yamada Y, Sato Y. XRD analysis of carbon stacking structure in coal during heat treatment. *Fuel*. 2004;83:2427–33.
40. Wu S, Gu J, Zhang X. Variation of carbon crystalline structures and CO<sub>2</sub> gasification reactivity of Shenfu coal chars at elevated temperatures. *Energy Fuel*. 2007;22:199–206.
41. Li RP, Zhang JL, Wang GW. Study on CO<sub>2</sub> gasification reactivity of biomass char derived from high-temperature rapid pyrolysis. *Appl Therm Eng*. 2017;121:1022–31.
42. Wang G, Zhang J, Hou X. Study on CO<sub>2</sub> gasification properties and kinetics of biomass chars and anthracite char. *Bioresour Technol*. 2015;177:66–73.
43. Shen BX, Liu DC, Chen HP. The kinetic parameters of petroleum coke pyrolysis and their compensating effect. *J Huazhong Univ Sci Technol*. 1999;27:36–7.
44. Yu RG, Chen Y, Lin C, Zhang JY. Catalytic gasification kinetics and compensation effect of high metamorphosed anthracite. *Combust Sci Technol*. 2012;18:85–9.